Petroleum Science 19 (2022) 3134–3148

Contents lists available at ScienceDirect

Petroleum Science

journal homepage: www.keaipublishing.com/en/journals/petroleum-science

Original Paper

Foaming supramolecular surfactants for gas mobility control in naturally fractured carbonate reservoirs at high temperature, salinity, and hardness

Enrique Soto-Castruita [a, b], Raúl Hernández-Altamirano [c], Eduardo Buenrostro-González [a], Erick-Emanuel Luna-Rojero [a], Sung Jae Ko-Kim [a], Violeta-Yasmín Mena-Cervantes [c], Mirna Pons-Jiménez [d], Jorge-Francisco Ramírez-Pérez [a], David-Aarón Nieto-Alvarez [a], Ricardo Cerón-Camacho [a, b], José-Ernesto Parra [a], Raúl Oviedo-Roa [a], José-Manuel Martínez-Magadán [a], Rodolfo Cisneros-Dévora [a, b, *], Luis-S. Zamudio-Rivera [a, **]

[a] Instituto Mexicano del Petróleo, Eje Central Lázaro Cárdenas Norte 152, Col. San Bartolo Atepehuacán, Ciudad de México, 07730, Mexico
[b] CONACyT-Instituto Mexicano del Petróleo, Eje Central Lázaro Cárdenas Norte 152, Col. San Bartolo Atepehuacán, Ciudad de México, 07730, Mexico
[c] Centro Mexicano para la Producción más Limpia, Instituto Politécnico Nacional, Avenida Acueducto s/n, Col. La Laguna Ticomán, Ciudad de México, 07340, Mexico
[d] Centro de Tecnologías para Exploración y Producción, Camino de Terracería 800, Col. San José Novillero, Boca del Río, Veracruz, 94286, Mexico

ARTICLE INFO

Article history:
Received 4 January 2022
Received in revised form
11 February 2022
Accepted 16 June 2022
Available online 21 June 2022

Edited by Jia-Jia Fei

Keywords:
Calcium chelation
Foaming composition
Supramolecular surfactant
Molecular design
Gas mobility control
Flow assurance
Improved oil recovery
Conformance control

ABSTRACT

Oil production and maintenance are essential issues in naturally fractured reservoirs because they are the largest and most productive on earth. However, they present early water and gas channeling but could be remediated by using foaming agents to control these phenomena through blocking channeling areas. In Mexico these reservoirs have pressure up to 5,500 psi, high temperature up to 200 °C, salinity up to 400,000 ppm, and hardness up to 250,000 ppm; due to these thermodynamic conditions, there has been no available technology to form stable enough foams. In this work, a foaming supramolecular surfactant with the capability to chelate Ca^{2+} ions is examined. As a result, surfactant monomers are bridged by captured Ca^{2+} cations leading to the formation of high-molecular-weight oligomers, which significantly increment the viscosity of the solution improving the foam stability, and since at this manner the Ca^{2+} cations are no longer available to precipitate as components of solid salts, the foaming supramolecular surfactant also performs as antiscalant. These observations are explained through quantum theoretical modeling. The foam is stable, effectively blocking the gas channels, whereas in presence of oil the foam is broken leading the oil to pass into the wellbore. The characteristic rheological properties of the foam allow its injection into the formation at a range of flow rates, foam qualities, and shear stress to achieve the flooding and the blocking of a variety of fractured carbonate formations, and the change of the wettability of the matrix, which is a desirable behavior in a *huff and puff* process, as reported in a previous publication about a successful pilot test of this foam.

1. Introduction

Maintaining and increasing oil production in naturally fractured reservoirs is a significant challenge (Kargarpour, 2020). These reservoirs are among the largest and most productive in the world (Bratton et al., 2022), because of their geological characteristics, such as the natural fractures and depths up to 6,000 m (Flores et al., 2011). For example, in the south and southeast regions of Mexico,

* Corresponding author. Instituto Mexicano del Petróleo, Eje Central Lázaro Cárdenas Norte 152, Col. San Bartolo Atepehuacán, Ciudad de México, 07730, Mexico.
** Corresponding author.
E-mail addresses: espercisneros@imp.mx (R. Cisneros-Dévora), lzamudio@imp.mx (L.-S. Zamudio-Rivera).

https://doi.org/10.1016/j.petsci.2022.06.013

oil reservoirs are naturally fractured and carbonated, with a low porosity for the formation but with preferential flow channels, due to fractures and dissolution cavities; also the rock wettability is towards oil, and temperatures in the order of 100–160 °C, salinities from 32,800 to 313,000 ppm, and hardness from 6,400 to 154,000 ppm of $CaCO_3$ (Hernández Altamirano et al., 2020). However, their production declines rapidly due to early gas or water channelings into the well (Wang and Sun, 2019), factors that make the oil recovery even more challenging (Parra et al., 2020a; Parra et al., 2020b; Xu et al., 2020). An alternative to manage this problem and improve the oil recovery factor is the use of chemicals to form foams that are able to control gas channeling; however, foam stability, at harsh conditions of temperature and pressure, decreases drastically (Bouquet et al., 2020; Xu et al., 2020; Chevallier et al., 2019; Hernandez Altamirano et al., 2016; Danzik, 1993; Rasheed et al., 1991). Li et al. (2018) used a gelled foam to increase the foam stability and to perform the conformance control in the reservoir fractures, based on a crosslinked foam that permanently blocks the high permeability channels that are good for a water flooding system but with the disadvantage to possibly generates permanent damage to the formation. More recently, works related to the use of foams at high temperature, salinity, and hardness, were presented in an international conference (AlYousef et al., 2020; Elhassan et al., 2019; Le et al., 2019; Skauge et al., 2019).

It is important to mention that by a definition, a supramolecular surfactant is a surfactant complex composed of small organic molecules or polymers having amphiphilic properties that self-assemble among them in a controlled way through non-covalent interactions (Zhang and Wang, 2011). In this research, we present two foaming supramolecular surfactants that preserve their foaming capacity under these conditions. The first supramolecular surfactant is based on betaine and has the capacity to retain its sodium ions while capturing the calcium ions, so the stability of the foam increases in comparison with the commercially available products. The second one is based on hydroxisultaine and has the same property to retain the sodium ions and capture the calcium, with the additional advantage that the hydroxy group works as a linker among surfactant molecules and leads to the formation of oil that increases viscosity, so the stability of the foam is increased too, this for harder conditions than the betaine based (Cisneros-Dévora et al., 2020; Sandrea, 2019; Mohamed et al., 2017; Hernandez Altamirano et al., 2016; Wu et al., 2016; Chen and Mohanty, 2014; Lu et al., 2014; Han et al., 2013). The second surfactant was successfully used for the generation of a stable foam at a pressure of up to ~5,500 psi, a temperature of up to ~200 °C, a salinity of up to ~400,000 ppm, and a hardness around of ~250,000 ppm of divalent ions (Pérez-Alvarez et al., 2018; Pons-Jiménez et al., 2015; Onoda et al., 2001). Furthermore, it had been already applied in a field test for gas mobility control in a reservoir having a temperature of 150 °C, 239,500 ppm of salinity as NaCl, and 125,000 ppm of hardness as $CaCO_3$. The pilot test was successfully evaluated by the Mexican oil operator (Flores-Mondragón et al., 2015). The test result demonstrated the viability of the FSS as the first available technology for gas mobility control in naturally fractured carbonate reservoirs at ultra-high conditions of temperature and salinity in the southeast region of Mexico.

2. Material and methods

The development of the FSS began through molecular design by using atomistic models to perform quantum-based calculations of interaction energies in the supramolecular complex. Next, the FSS was synthesized and their performance was tested in the laboratory as described in the following sections.

2.1. Quantum modeling

2.1.1. Molecular modeling

For the quantum computational molecular design of the foaming agents, four raw surfactants were modeled: (a) sodium (*E*)-non-2-ene-1-sulfonate (SENES, Fig. 1), (b) sodium (3-hydroxinonane-1-sulfonate (SHNS, Fig. 1), (c) 2-[3-(nonanoylamidopropyl)-dimethylazaniumyl]acetate (NAAA, Fig. 1), which is a betaine-based surfactant, and (d) 3-[(3-nonanoylamidopropyl)dimethylazaniumyl]-2-hydroxypropane-1-sulfonate (NAAHS, Fig. 1), which is a sultaine-based surfactant. By using them, supramolecular monomers FSS(α) (Fig. 1e) and FSS(β) (Fig. 1f) having 1:1:2 stoichiometric ratios of SENES, SHNS, and NAAA (for FSS(α)) or NAAHS (for FSS(β)) were built, according to the reactions below:

$$\text{SENES} + \text{SHNS} + 2\ \text{NAAA} \rightarrow \text{FSS}(\alpha) \quad (1)$$

$$\text{SENES} + \text{SHNS} + 2\ \text{NAAHS} \rightarrow \text{FSS}(\beta) \quad (2)$$

Likewise, it was built the molecular models of two premicelles FSS(ℓ):$CaCl_2$:FSS(ℓ, where ℓ is α or β (Fig. 2b and 2c, respectively), each one formed by a FSS dimer whose monomers are linked between them by hydrogen bonds and by a unit of calcium chloride ($CaCl_2$), *i.e.*, the $CaCl_2$:FSS stoichiometric ratio is 1:2. Finally, a 2:3-stoichiometric bigger premicelle FSS(β):$CaCl_2$:FSS(β):$CaCl_2$:FSS(β) was built to model the formation of oligomeric structures formed by fusion of supramolecular monomers (Fig. 2d). The reactions for the formation of each of these supramolecular complexes are the following:

$$CaCl_2 + 2\ \text{FSS}(\alpha) \rightarrow \text{FSS}(\alpha):CaCl_2:\text{FSS}(\alpha) \quad (3)$$

$$CaCl_2 + 2\ \text{FSS}(\beta) \rightarrow \text{FSS}(\beta):CaCl_2:\text{FSS}(\beta) \quad (4)$$

$$2\ CaCl_2 + 3\ \text{FSS}(\beta) \rightarrow \text{FSS}(\beta):CaCl_2:\text{FSS}(\beta):CaCl_2:\text{FSS}(\beta) \quad (5)$$

In Figs. 1 and 2, all the final conformations of the molecules associated with the minimum energy value are shown. Observing in each case that the supramolecular monomers, as well as, the premicelle emphasize the affinity between aliphatic chains and the polar groups of the raw materials with the dissolved ions, which generates stable structures.

2.1.2. Quantum computational calculations

All above molecular models were built using the Materials Studio (MS) interface (Accelrys Software Version 7.0 Inc, 2012). In particular, the DMol3 module was used to perform the Density Functional Theory calculations in a water environment through the conductor-like screening model (COSMO) using the dielectric constant of water, 78.54 (Klamt and Schüürmann, 1993). Molecular geometry optimizations were obtained by minimizing the total electronic energy of all molecular and supramolecular models through DMol3 runs, which were performed by using the local density approximation (LDA) functional developed by Vosko-Wilk-Nusair (VWN) (Vosko et al., 1980), the OBS correction for dispersions (Ortmann et al., 2006), the effective core potentials for core treatment (Bergner et al., 1993; Dolg et al., 1987), unrestricted spins, and the basis set DNP. All remaining run parameters were set at the coarse accuracy option.

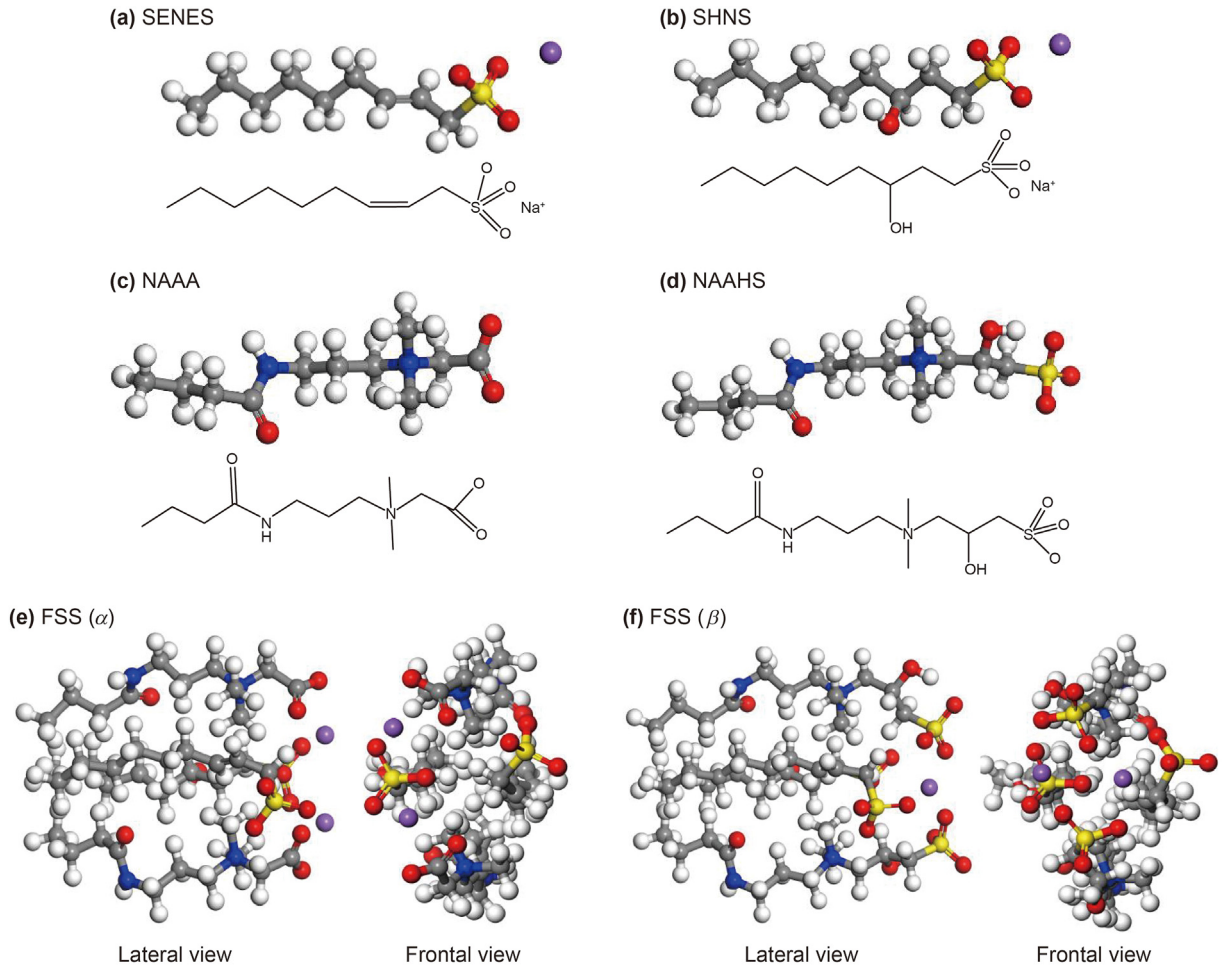

Fig. 1. Atomistic molecular models for **(a)** sodium (*E*)-non-2-ene-1-sulfonate ($C_9H_{17}O_3NaS$), **(b)** sodium (3-hydroxinonane-1-sulfonate ($C_9H_{19}O_4NaS$), **(c)** 2-[3-(nonanoylamidopropyl)-dimethylazaniumyl]acetate (betaine based surfactant) ($C_{11}H_{22}N_2O_3$), **(d)** 3-[(3-nonanoylamidopropyl)dimethylazaniumyl]-2-hydroxypropane-1-sulfonate (sultaine based surfactant), and the supramolecular monomers ($C_{12}H_{26}N_2O_5S$), **(e)** FSS(α) and **(f)** FSS(β). Atom's colors stand for hydrogen (white), sulfur (yellow), carbon (grey), oxygen (red), nitrogen (blue) and sodium (purple).

The viability for the formation of each of the supramolecular complexes, according to reactions from Eqs. (1)–(5), was quantified by calculating the interaction energy ΔE_{int} as below:

$$\Delta E_{int} \equiv E_{SC} - \sum E_R \tag{6}$$

where E_{SC} is the total electronic energy of a supramolecular complex and $\sum E_R$ is the sum of the total electronic energies of its reactants, respectively.

2.2. Experimental methodology

2.2.1. Materials

All used reagents were industrial grade. All FSSs mentioned in section 2.1 were prepared using the corresponding commercially available materials: a mixture of sodium (*E*)-dodec-2-ene-1-sulfonate/sodium 3-hydroxydodecane-1-sulfonate; 2-[3-(dodecanoylamidopropyl)-dimethylazaniumyl] acetate as the betaine based surfactant; and 3-[(3-dodecanoylamidopropyl)dimethylazaniumyl]-2-hydroxypropane-1-sulfonate as the sultaine based surfactant. The commercial cationic foaming agent (CCFA), commercial anionic foaming agent (CAFA), and commercial zwitterionic foaming agent (CZFA) were provided by Stepan Chemical Co.

The physicochemical characterization of the connate waters and crude oil from reservoirs located in the southeast of Mexico, used for the performance tests, are shown in Table 1.

2.2.2. Synthesis of FSSs

The FSSs were synthesized in stoichiometric amounts (according to Section 2.1.1) and characterized by FT-IR and NMR experiments, according to the established method reported in the patents US8722588B2 and US9469804B2 (Hernandez Altamirano et al., 2016; Zamudio Rivera et al., 2014), and used dissolved at 30% in water.

It is worthy to mention that the lab-obtained FSSs (Fig. 3) slightly vary from the theoretically modeled FSSs (Fig. 1) in that the tails of their components are 3 carbons longer; that is, FSS(α) is the stoichiometric mixture of 2-[(3-dodecanoylamidopropyl)dimethylazaniumyl] acetate (DAAA in Fig. 3c, which is the betaine based surfactant), sodium (*E*)-dodec-2-ene-1-sulfonate (SEDES in Fig. 3a) and sodium 3-hydroxydodecane-1-sulfonate (SHDS in Fig. 3b) within the water, whereas FSS(β) is the stoichiometric mixture of 3-[3-(dodecanoylamidopropyl)-dimethylazaniumyl]-2-hydroxypropane-1-sulfonate (DAAHS in Fig. 3d, which is the hydroxysultaine based surfactant), SEDES and SHDS in water.

2.2.3. FT-IR and NMR

FT-IR spectra were recorded on an IR Smith HAzMathID 360

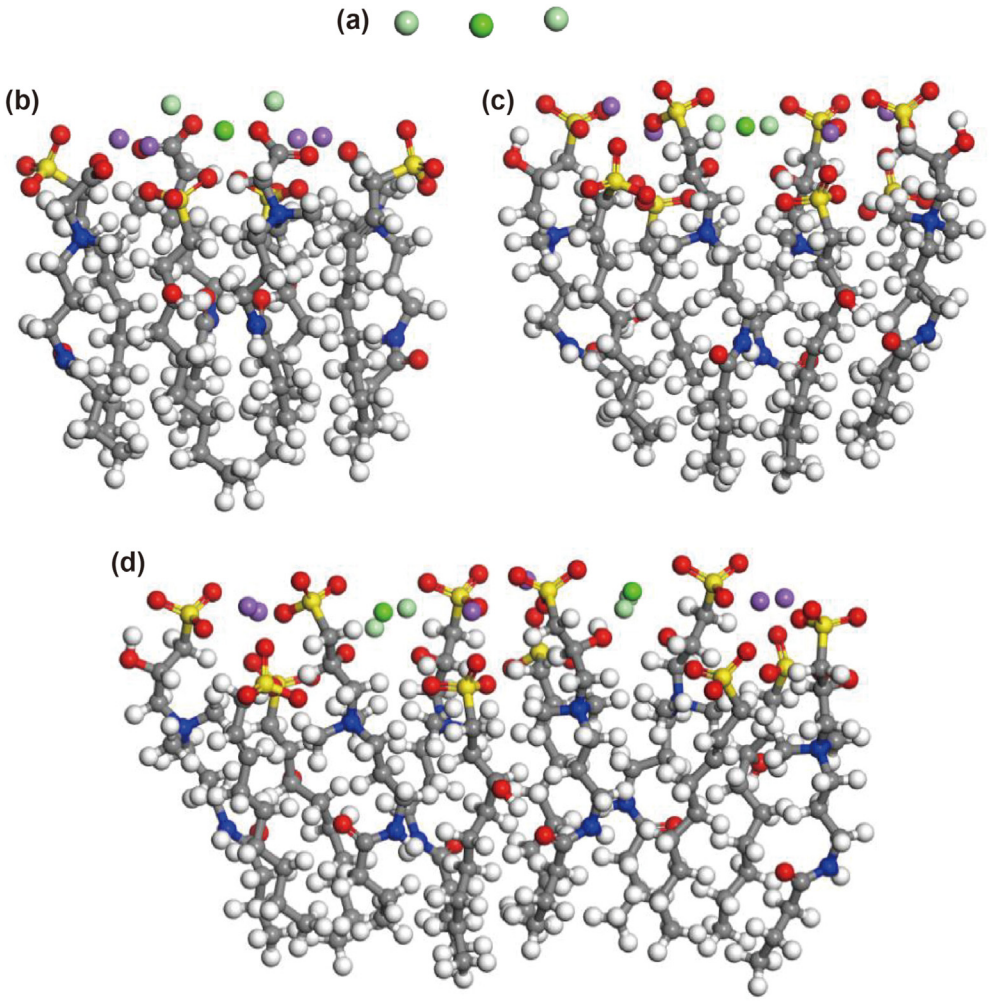

Fig. 2. Atomistic molecular models for **(a)** a unit of $CaCl_2$, **(b)** the premicelle FSS(α):$CaCl_2$:FSS(α), **(c)** the premicelle FSS(β):$CaCl_2$:FSS(β), and **(d)** the oligomer FSS(β):$CaCl_2$:FSS(β):$CaCl_2$:FSS(β). Atom's colors stand for chlorine (light green) and calcium (dark green).

using the ATR mode; the observed bands correspond to those reported in the mentioned patents. All NMR spectra ^{1}H and ^{13}C were performed on a Bruker Advance III 300 spectrometer in $CDCl_3$. Chemical shifts (δ) are in ppm and referenced to the TMS peak.

Table 1
Physicochemical characterization of seawater, connate water 1, connate water 2, and three crude oils.

	Seawater	Connate water 1	Connate water 2
Salinity as NaCl, ppm	32,803.9	152,974.9	253,859.1
Hardness as $CaCO_3$, ppm	6,420	35,200	87,700
Na^+, ppm	11,742.00	44,223.39	59,809.50
Ca^{2+}, ppm	448	12,720	31,880
Mg^{2+}, ppm	1,288.40	826.54	1,944.80
Sr^{2+}, ppm	6.9	710.0	1,450.0
Ba^{2+}, ppm	0.20	1.84	25.30
Cl^-, ppm	19,900	92,800	154,000
SO_4^{2-}, ppm	3,650	225	300
CO_3^{2-}, ppm	13.2	0.0	0.0
HCO_3^-, ppm	84.20	256.20	148.84
	Crude oil 1	**Crude oil 2**	**Crude oil 3**
Saturates, wt%	18.7	31.88	38.32
Aromatics, wt%	31.8	48.84	45.98
Resins, wt%	37.8	18.81	15.63
Asphaltenes, wt%	11.7	0.38	0.07
Acid number, mg KOH/g	0.5	0.29	0.14
Basic number, mg KOH/g	–	1.33	0.40

2.2.4. Foaming evaluation at atmospheric and reservoir conditions

The performance of a commercial surfactant, the betaine based supramolecular surfactant FSS(α), and the sultaine based supramolecular surfactant FSS(β) was evaluated at atmospheric and reservoir conditions in a 50 mm internal diameter and 1 m total height cylindrical container of borosilicate (Fig. 4), which has a heating jacket feeding with a thermal fluid for temperature control, a gas injection stainless steel line with 5 mm of diameter located inside its interior, and a diffuser with a 0.5 mm of mean pore diameter at atmospheric pressure and 70 °C, located 50 mm from the bottom. Also, 60 mL of the sample prepared with seawater or connate water (Table 1) containing 2,000 ppm of either a commercial or supramolecular surfactant was placed in the container at a temperature of 70 °C. Then, it was injected nitrogen at a flow rate of 50 mL per minute for 45 s. At this moment, the foam height was measured from the foam-liquid interface to the foam-air surface every 10 min, until reduced down to less than 30% of the initial value.

The foam stability is calculated according to the following equation:

$$Foam\ stability = \frac{H_T - H_S}{(H_T - H_S)_{max}} \tag{7}$$

where, H_T is experiment total height and H_S is the liquid-solution

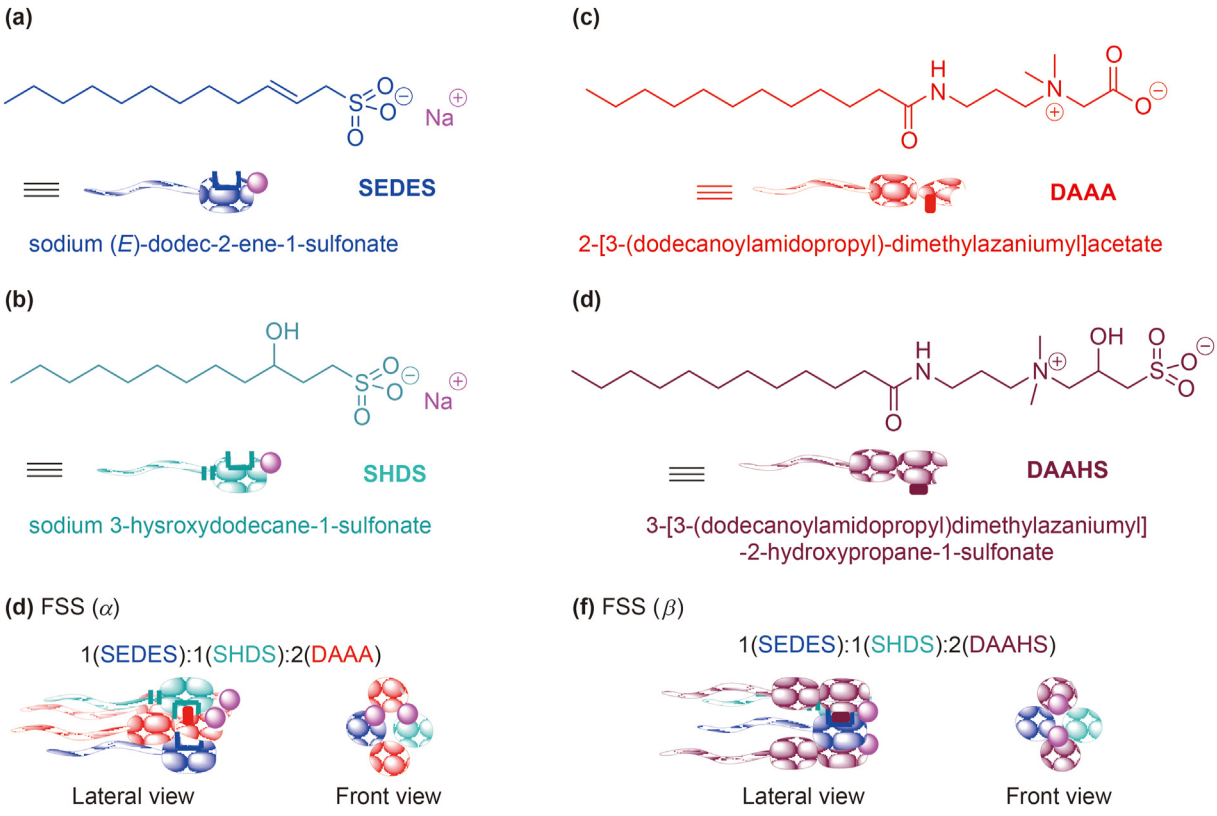

Fig. 3. Schemes of the experimentally synthesized supramolecular surfactants FSS(α) and FSS (β).

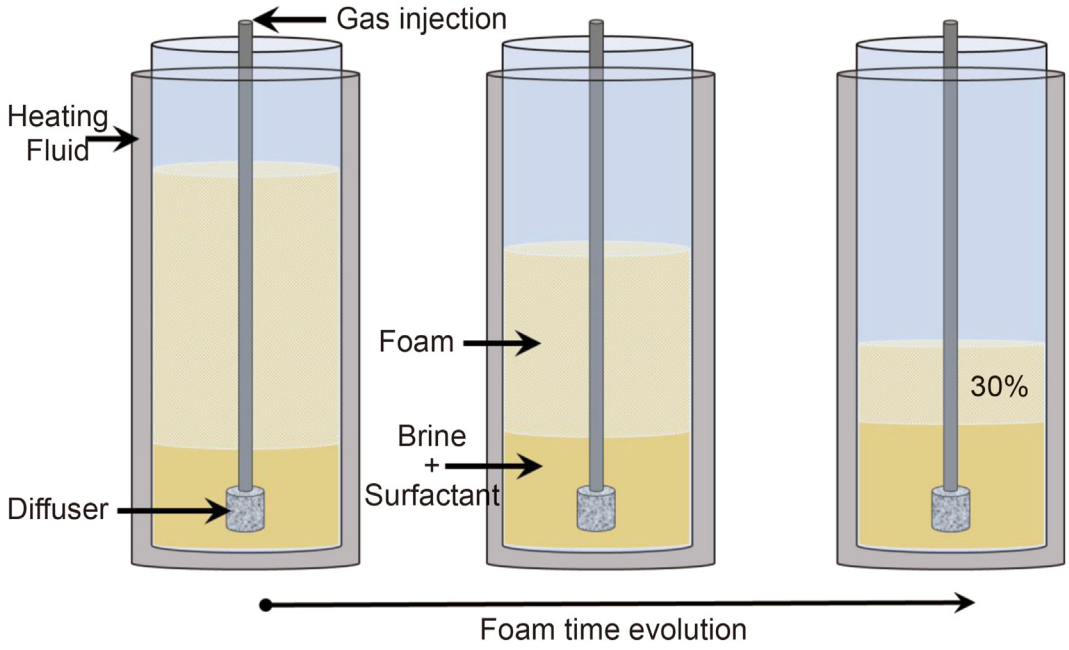

Fig. 4. Chamber for the foam generation and stability determination at atmospheric pressure and controlled temperature.

height.

A similar device was built to study the foam formation and stability at reservoir conditions (Fig. 5). In this case, the container is a stainless steel square chamber with 8 cm per side and a height of 25 cm. It has a diffuser in the bottom through which the gas is injected in the high-pressure chamber at 160 °C and 3,500 psi.

2.2.5. Rheological measurements

The rheological measurements at reservoir conditions were carried out in a capillary rheometer having a foam generator, developed at Instituto Mexicano del Petróleo. The temperature and inner pressure of the rheometer were set up to 150 °C and 3,500 psi, respectively. The brine with or without supramolecular surfactant

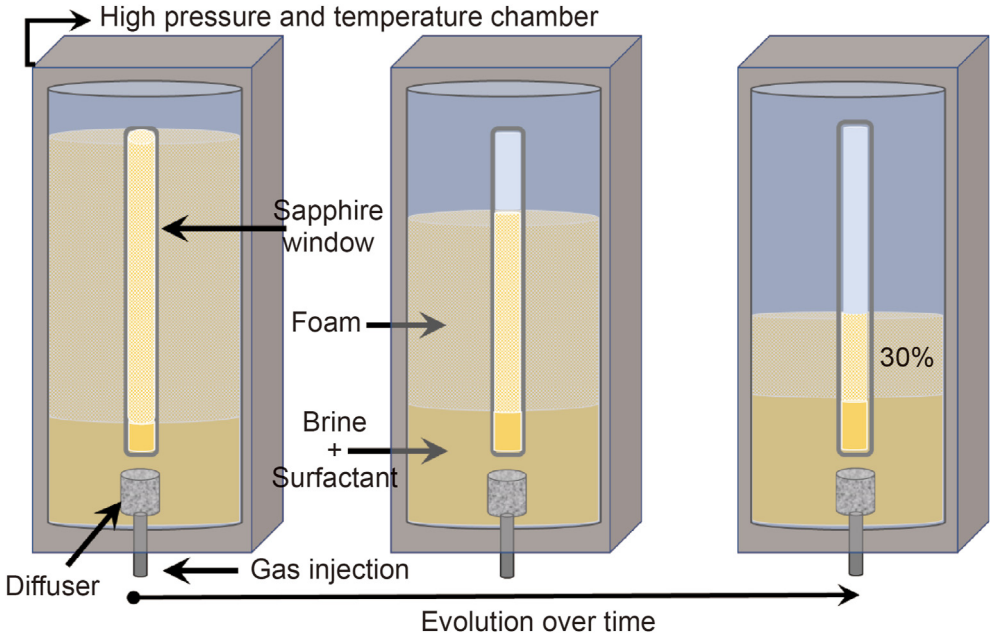

Fig. 5. Device for the foam generation and stability determination at reservoir pressure and temperature conditions.

was injected into the capillary by using a high-pressure positive-displacement pump at a controlled flow rate. In contrast, the nitrogen gas was injected in the same line from a pressurized tank at 5,000 psi. The gas flow rate was determined by calculating the foam quality according to the equation:

$$Foam\ quality = \frac{Q_g}{Q_g + Q_S} \tag{8}$$

where Q_g and Q_S are the flow rate of the gas and of the liquid solution, respectively. It is worthy to mention that by considering $Q_g = \Delta V_g/\Delta t$ and $Q_s = \Delta V_s/\Delta t$, where ΔV_g and ΔV_s are the gas and oil volumes displaced within the time interval Δt, the foam quality is equivalent to the gas oil ratio $\Delta V_g/(\Delta V_g + \Delta V_s)$.

2.2.6. Core flood experiments

Experimentally, fluid flow in porous rocks is commonly investigated by core flood experiments. These experiments are widely used in petroleum engineering to investigate miscible and immiscible fluid displacement and to understand subsurface flow to maximize oil recovery.

Core flood experiments were performed to determine the gas flow blocking or resistance factor that the foam can generate. This factor was determined at irreducible water saturation core condition, either under the presence or absence of oil.

A longitudinally fractured cylindrical sample of Bedford limestone was used to simulate the flow in a fractured medium; the sample and its geometrical parameters are described in Fig. 6.

The rock sample is placed in a vertical core holder (Fig. 7) and is subjected to confining pressure. Solution injection was performed through the longitudinal direction. A pressure control valve was placed at the system exit to achieve the desired fluid pressure inside the core. Pressure in both the inner and exit faces was measured with pressure transducers, the temperature was measured through a thermocouple, and the data were recorded on a computer.

The oil saturation of the core was performed at reservoir conditions and monitored until the core differential pressure was constant, while the oil injection flow rate was 1.0 mL/min. These conditions were achieved after 4 pore volumes of injected oil.

2.2.7. Interfacial measurements

Interfacial tension was measured through the pendant drop method. It involves determining the profile of a drop of a fluid in suspended mechanical equilibrium in another fluid. Fig. 8 shows the profile that the pending drop must meet and the variables considered to determine the interfacial tension τ:

$$\tau = (\rho_A - \rho_B)gdD, \tag{9}$$

where D is the diameter of the largest length within the sloping droplet, d is the resulting diameter of the drop neck at the distance D measured from the drop bottom to the neck, ρ_B is the density of the fluid with lower density, and ρ_A is the density of the fluid with the highest density.

3. Results and discussion

3.1. Theoretical results

The formation of both supramolecular monomers FSS(α) and FSS(β) (Fig. 1e and 1f, respectively) are thermodynamically favorable because the interaction energies among their components are negative (Table 2). These supramolecular monomers are very similar; the differences are the betaine-based surfactant NAAA in FSS(α) and the hydroxysultaine-based surfactant NAAHS in FSS(β), which have the same tails but different heads. Since the hydroxyl and sulfonate groups confer more polarity to the hydroxysultaine head than the carboxylate group does to the betaine head, NAAHS tends to be more dissolved than NAAA by the polar aqueous environment. That is, under water, FSS(β) must be less stable than FSS(α), as it is revealed by their interaction energies: $|\Delta E_{int}(FSS(\beta))| < |\Delta E_{int}(FSS(\alpha))|$ (Table 2).

However, the high polarity of the hydroxysultaine-based surfactant is just what allows the supramolecular monomer FSS(β) to bind a Ca^{2+} cation more intensively than the supramolecular monomer FSS(α), containing the less-polar betaine-based

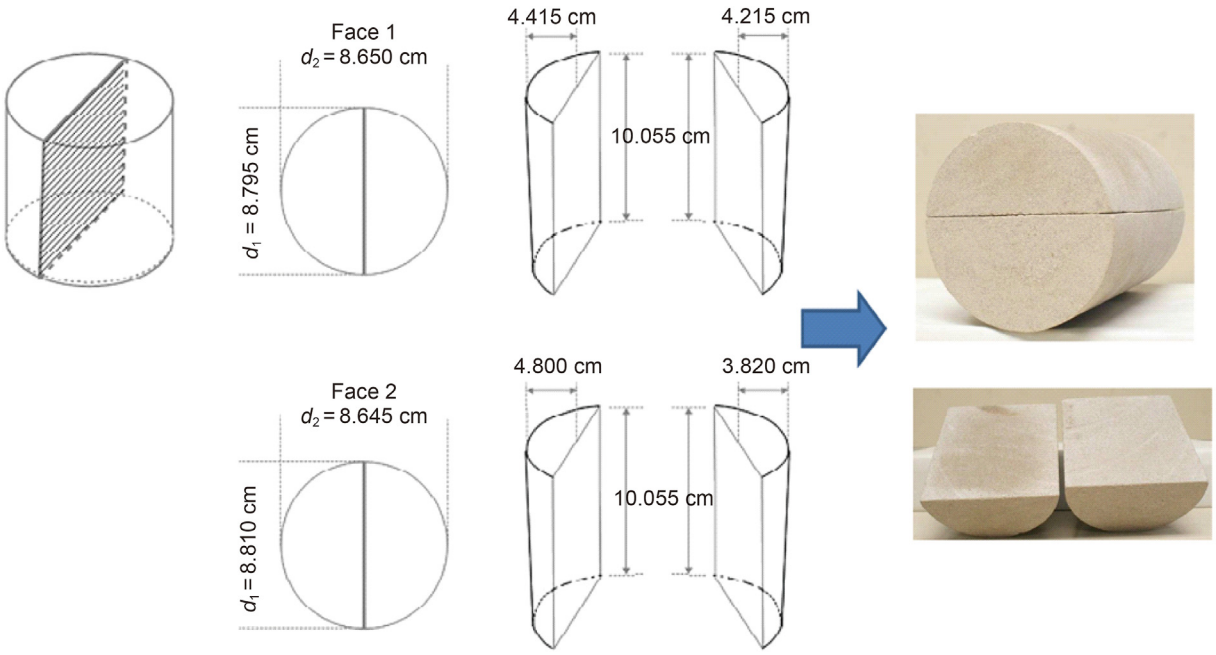

Fig. 6. Dimensions of the longitudinally fractured Bedford limestone core.

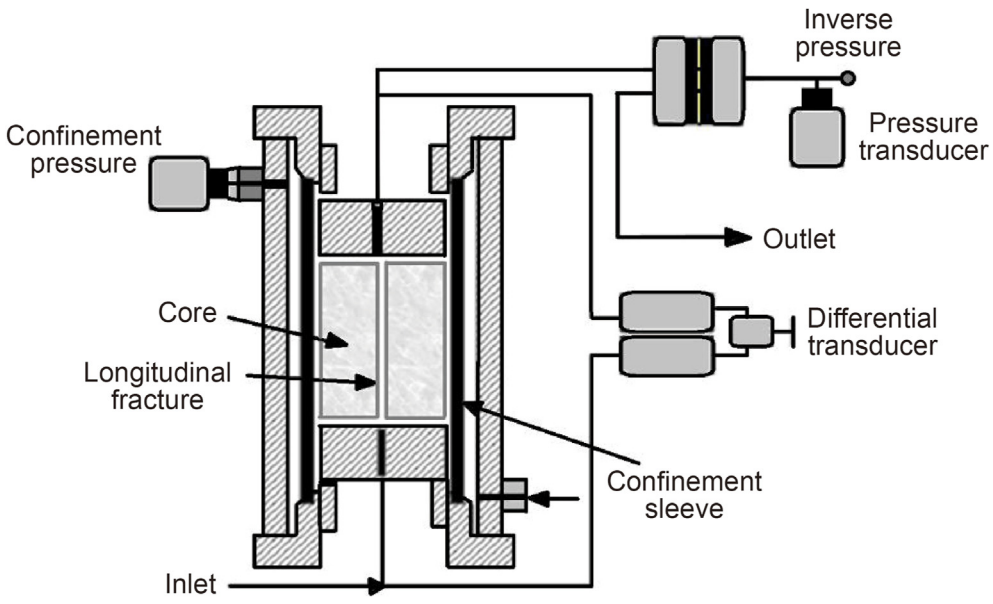

Fig. 7. Core holder and peripheral devices are used to determine the flow behavior in fractured media.

surfactant, does (− 341.20 vs. − 295.96 kcal/mol, respectively see Table 2 and Fig. 2b and 2c). The Ca^{2+} cation links to either two betaine-based surfactants or two hydroxysultaine-based surfactants because of the unitary negative formal charge of the carboxylate and sulfonate groups, respectively, which facilitate the formation of premicelles of the supramolecular monomers FSS(α) or FSS(β). Nevertheless, the hydroxylic oxygens of the hydroxysultaine-based surfactants also are attracted by Ca^{2+}; then, each of the two surfactants NAAHS forms a 6 membered chelate ring with the Ca^{2+} cation (Fig. 9) through 2 coordinate oxygens. It is worthy of mentioning that all four O···Ca distances (from 2.24 to 2.44 Å, Fig. 9) are around the sum (2.39 Å) of the ionic radii of oxygen (1.40 Å) and calcium (0.99 Å) (LENNTECH, 2022), confirming that Ca^{2+} forms coordinate bonds with these oxygens; moreover, these O···Ca bond distances are consistent with results from the literature (Gagné and Hawthorne, 2016). The resulting double chelate (Fig. 9) leads to the strongest interaction energy inside the premicelle FSS(β):$CaCl_2$:FSS(β) $\beta\alpha$(Fig. 2c), in contrast to the absence of chelates in the premicelle FSS(α):$CaCl_2$:FSS(α) (Fig. 2b). Further growing of premicelles of FSS(β) to form oligomers, as in the reaction of Eq. (5) and Fig. 2d, is thermodynamically favorable (see Table 2), which is a convenient fact to get stable foam lamellas. Thus, the presence of divalent ions in the aqueous environment induces the formation of premicelles of FSSs supramolecular monomers, and if these FSSs monomers contain hydroxysultaine-based surfactants, the premicelles will be more

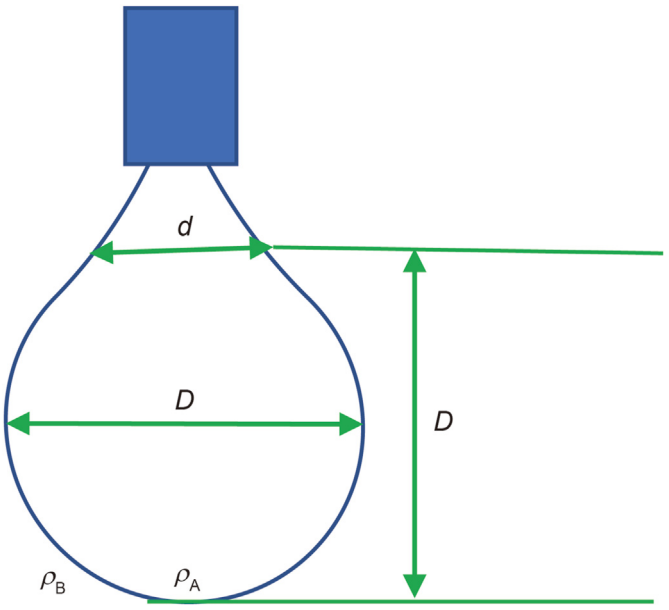

Fig. 8. Schematic representation of a drop with the geometrical parameters used to determine the interfacial tension.

Table 2
Total electronic energy E_R of the reactants and E_{SC} of the supramolecular complexes (Figs. 1 and 2), and interaction energies ΔE_{int} for latter. Energy units in kcal/mol.

Reactants		E_R
$CaCl_2$		− 999,931.95
SENES		− 710,807.30
SHNS		− 758,491.60
NAAA		− 477,889.43
NAAHS		− 845,964.28
Supramolecular complex	E_{SC}	ΔE_{int}
FSS(α) supramolecular monomer	− 2,425,365.04	− 287.29
FSS(β) supramolecular monomer	− 3,161,484.99	− 257.55
FSS(α):$CaCl_2$:FSS(α) premicelle	− 5,850,957.99	− 295.96
FSS(β):$CaCl_2$:FSS(β) premicelle	− 7,323,243.13	− 341.20
FSS(β):$CaCl_2$:FSS(β):$CaCl_2$:FSS(β) oligomer	− 11,484,816.66	− 497.79

stable. This prediction is confirmed in the experimental Section 3.3 below.

3.2. Synthesis and characterization

After the theoretical results, the first step was the synthesis and posterior characterization of the FSSs. In Fig. 10 are the corresponding FT-IR spectra for the characterization of FSS(β); at the top are the spectra for DAAHS component and exhibit bands in 1632 cm^{-1} for carbonyl group; in 1189 and 1038 cm^{-1} corresponding to sulfonate group. On the other hand, the middle spectra for mixture 1:1 SEDES/SHDS exhibit 1636 cm^{-1} for double bond; 1170 and 1042 cm^{-1} correspond to sulfonate groups. Finally, bottom spectra correspond to FSS(β): for carbonyl group initially appears in 1632 cm^{-1} in DAAHS and now appears in 1635 cm^{-1} with a displacement of 3 cm^{-1}. Bands corresponding to sulfonate groups now appear in 1177 and 1040 cm^{-1} showing a shift of 7 and 2 cm^{-1} concerning the band on SEDES/SHDS. Due to the large displacement of the vibration frequencies of the sulfonate bands concerning the raw materials, appear to be evidence of the supramolecular interaction between sulfonate groups on FSS(β). These displacements in FT-IR (Fig. 10) have been studied and evidenced in several scientific articles as proof that a supramolecular assembly has occurred. (Donon et al., 2021; Schalley, 2007). For FSS(α), also is observed similar displacements on the corresponding bands. Fig. 11 shows the interactions between sulfonate and carbonyl groups for FSS(α) and interactions between sulfonate groups on FSS(β) discussed by FT-IR.

Through Nuclear Magnetic Resonance (NMR) technique, supramolecular assemblies can be characterized by the variation in the chemical shifts (δ) of the corresponding functional groups with respect to the original raw materials (Grant, 2002). Fig. 12 shows a representative zoom of the ^{13}C-NMR spectra of FSS(β). At the top, for the mixture SEDES/SHDS, the corresponding signal for C—OH appears in 72.67 ppm, and C—SO_3^- appears in 57.35 ppm. For the DAAHS spectra, carbonyl signal appears at 177.88 ppm, the sign of C—OH appears in 74.26 ppm, signal C—N^+ in 69.30 ppm, C—SO_3^- in 64.96 ppm, N^+Me_2 in 64.69 ppm. Finally, FSS(β) exhibits displacements of the signal with respect raw materials. For example, the signal for C—OH in FSS(β) appears in 74.70 ppm with a displacement of 2.030 ppm; also, the signs of C—N^+ and C—SO_3^- and N^+Me_2 appears now at 69.89, 65.38, and 65.12 ppm, respectively. Also, the signal for C—SO_3^- that initially seems at 57.35 ppm appears

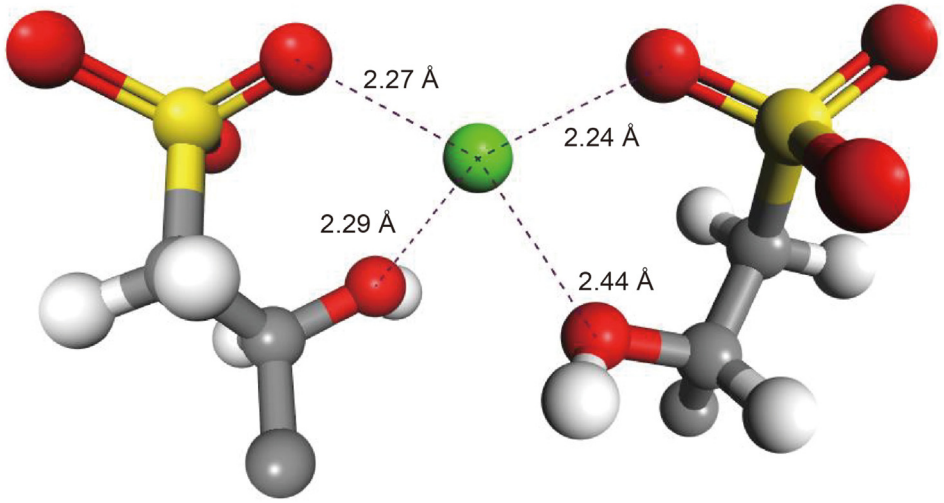

Fig. 9. Close view of the double chelate formed by two supramolecular monomers FSS(β)s with a Ca^+ cation.

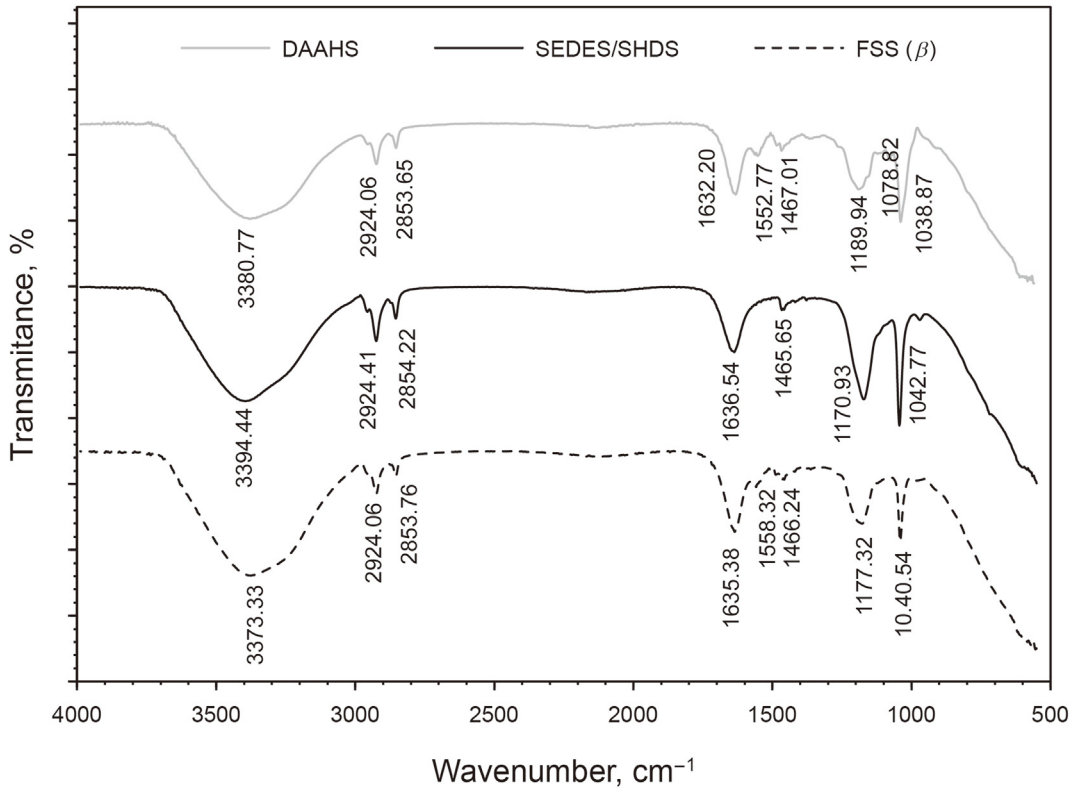

Fig. 10. IR spectra for DAAHS (top), mixture 1:1 of SEDES/SHDS (middle) and FSS(β) (bottom).

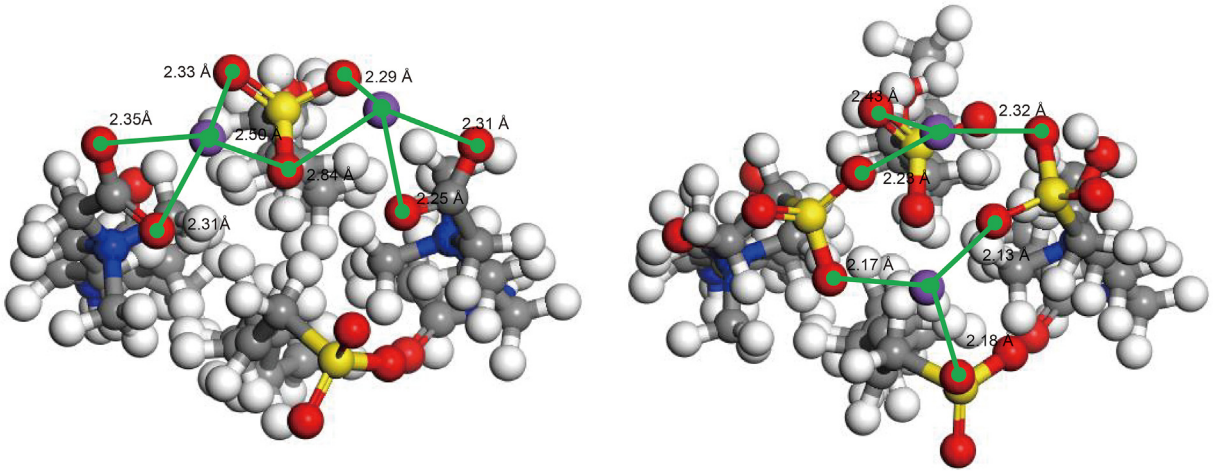

Fig. 11. Supramolecular interactions between the carbonyl sulfonate chemical groups for FSS(α) (left) and interactions sulfonate-sulfonate groups for FSS(β) (right), the lines indicate the distance in angstroms.

at 57.78 ppm in the supramolecular surfactant. Similarly, FSS(α) shows the corresponding shifts according to reported in the patent US8722588B2 (Hernandez Altamirano et al., 2016; Zamudio Rivera et al., 2014).

These variations in chemical shifts (δ) in NMR evidence supramolecular assemblies between SEDES:SHDS:2DAAHS that form FSS(β) through the interaction between sulfonate and carbonyl, and −OH groups present on the raw materials. This information is according to discussed and founded by FT-IR.

3.3. Foaming stability

The results of the foam stability test for the commercial, betaine based, and sultaine based compounds show that the CCFA, CAFA, and CZFA form the less stable foams since the latter last around 1 h (Fig. 13). These commercial agents are characterized by containing alfa olefin sodium sulfonates, which are susceptible to losing their sodium ions forming calcium salts with moisturizing properties, instead of the required foaming properties. On the contrary, foam

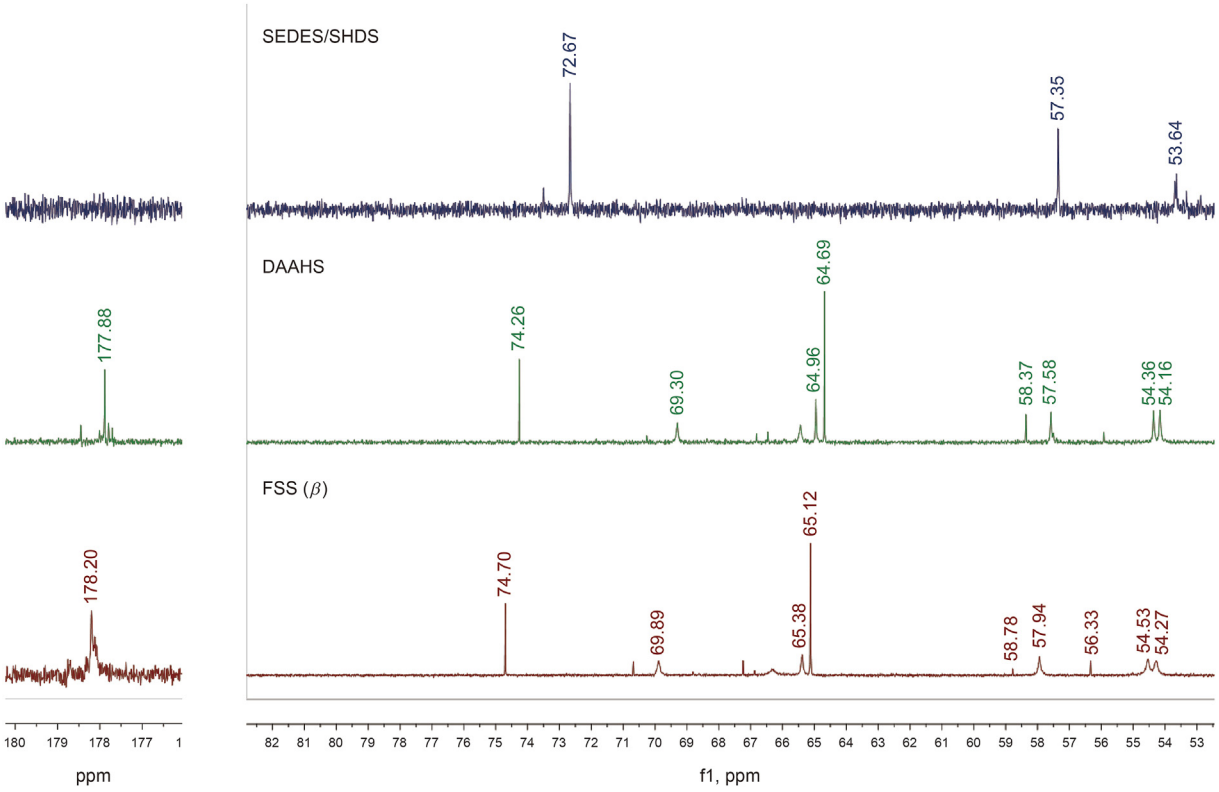

Fig. 12. ^{13}C-NMR spectra for the 1:1 mixture between the components SEDES and SHDS (top), the component DAAHS (middle), and FSS(β) (bottom).

stability increases to more than 2 h for the case of FSS(α) due to the supramolecular structure based on betaine, which does not exchange the sodium ions and consequently is able to form foams in the presence of the calcium ions at the reservoir conditions. For its part, FSS(β), which is based on sultaine, in addition, to retain the sodium ion while it captures the calcium ion, can link surfactants molecules among themselves, through the hydroxy group, and form oligomers, it leads to an increase of the viscosity, and generates foams with higher stability (more than 5 h) at the salinity and hardness conditions (Hernandez Altamirano et al., 2016). From this experiment, it can be observed that the sultaine based compounds can form stable foams under reservoir conditions (Zhang et al., 2003).

From a chemical point of view, the FSS(β)'s performance is explained by the well-known fact that the hard cation Ca^{2+} prefers to link harder anions having a high oxygen content (Katz et al., 1996), such as carboxylates and sulfonates. However, with carboxylate derivatives, it is possible only to form mono-dentate or bi-dentate coordination complexes. In contrast, sulfonate groups have higher oxygen content in comparison with carboxylate derivatives. Moreover, sulfonate groups permit the formation of sulfonate-bridged metal centers due to their coordinative capability to generate networks (Liu et al., 2016; Côté and Shimizu, 2001). Likewise, crystal structures have demonstrated the polymeric coordination of the sulfonate group in the presence of Ca^{2+} ions, where each Ca^{2+} unit is coordinated to two sulfonates of different ligands, forming a one-dimensional chain (Onoda et al., 2001).

Besides, from the theoretical point of view, it has been demonstrated that sulfonate groups from supramolecular complexes, in the presence of Ca^{2+} ions, give rise to the formation of supramolecular aggregates, *i.e.*, the Ca^{2+} cation drives the self-assembly (Zamudio Rivera et al., 2014). Also, there is evidence that supramolecular surfactants having sulfonate groups possess better performance in capturing Ca^{2+} ions with respect to the supramolecular surfactants having carboxylate groups. Then, supramolecular surfactants containing the sulfonate group could form aggregates of higher molecular weight due to the coordination provided by Ca^{2+} ions present in connate waters (Pérez-Alvarez et al., 2018; Pons-Jiménez et al., 2015). Incorporating Ca^{2+} in the supramolecular aggregate explains the high foam stability associated with the increase of the continuous phase viscosity.

In agreement with the theoretical molecular design, the stability-test results confirm the FSS(β) supramolecular complex generates stable foams in hardness waters (Fig. 14), where it is observed that the foams are more stable as the concentration of divalent ions is higher, *i.e.*, the divalent ions favor the foaming capacity of the supramolecular surfactant.

In addition, the reservoir conditions of high temperature and high pressure favor the stability of the foams even more (Amro et al., 2015; Firoze Akhtar et al., 2018; Wang et al., 2017), as observed in Fig. 15. Chemically the higher stability of the foam at high pressure and temperature is attributed to an increase in the mobility of the Ca^{2+} cations, due to the increase in kinetic energy, among the long hydrocarbon tails of the surfactant components, so it was easier to contact with the polar heads and so it was easier to activate the formation of oligomers. In other words, to form the oligomer is necessary that the ions and the polar heads match themselves; the increase in temperature increases ion mobility, and then the probability to form the oligomer increases too.

3.4. Interfacial tension

In Fig. 16, the drops generated at reservoir conditions of 150 °C and 2,000 psi with connate water 1 and crude oil 1 (Table 1), without and with FSS(β) at 600 ppm, are presented. It is worth

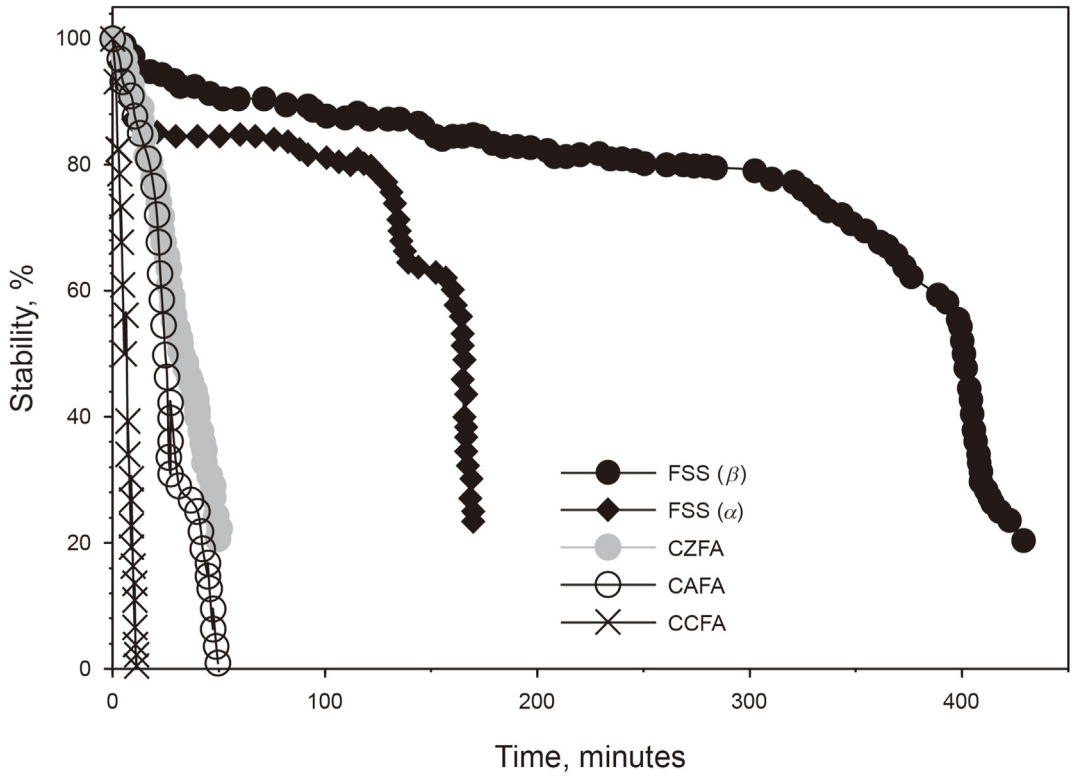

Fig. 13. Foam stability for FSS(β), FSS(α), CZFA, CAFA and CCFA.

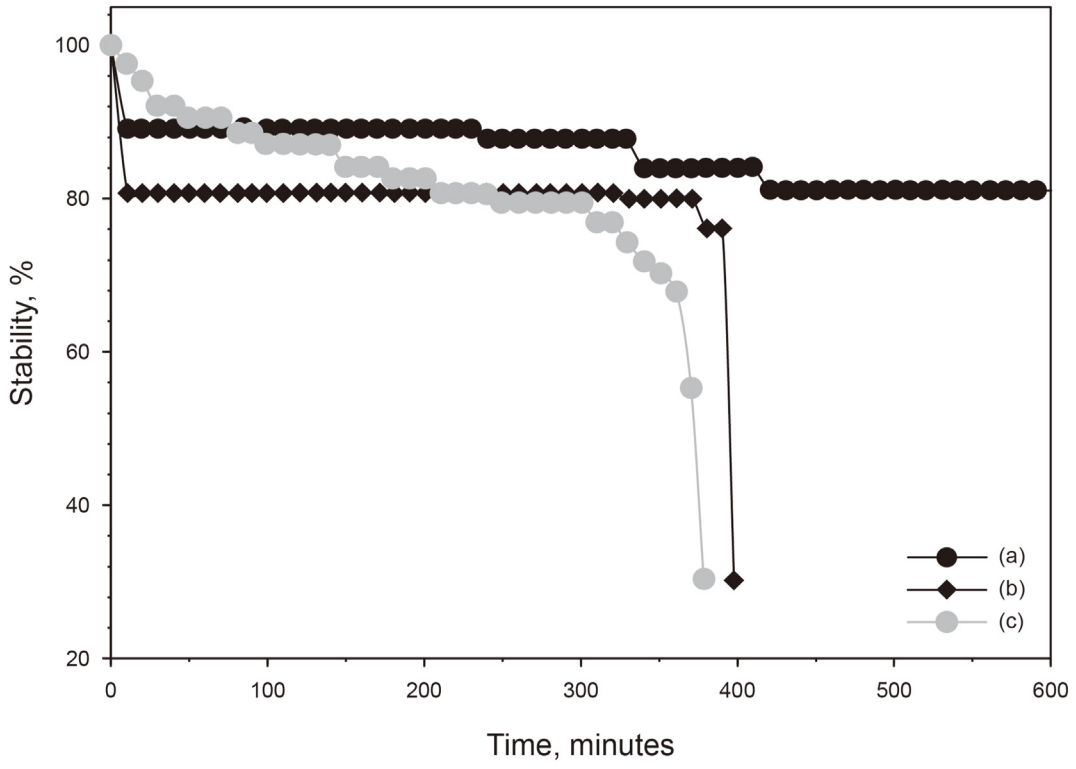

Fig. 14. Stability of foams produced by 200 ppm of FSS(β) dissolved in the brines shown in Table 1, at 70 °C and under atmospheric pressure: (a) connate water 2 (248,000 NaCl ppm, 135,000 $CaCO_3$ ppm, (b) connate water 1 (260,000 NaCl ppm, 87,700 $CaCO_3$ ppm), and (c) seawater (37,100 NaCl ppm, 6,400 $CaCO_3$ ppm).

observing that, in both cases, the drops are stabilized in the brine, this fact is important because means that the supramolecular surfactant does not promote the self emulsification phenomena under reservoir conditions which is a no desirable effect in the gas control mobility.

The interfacial tension value for the system without

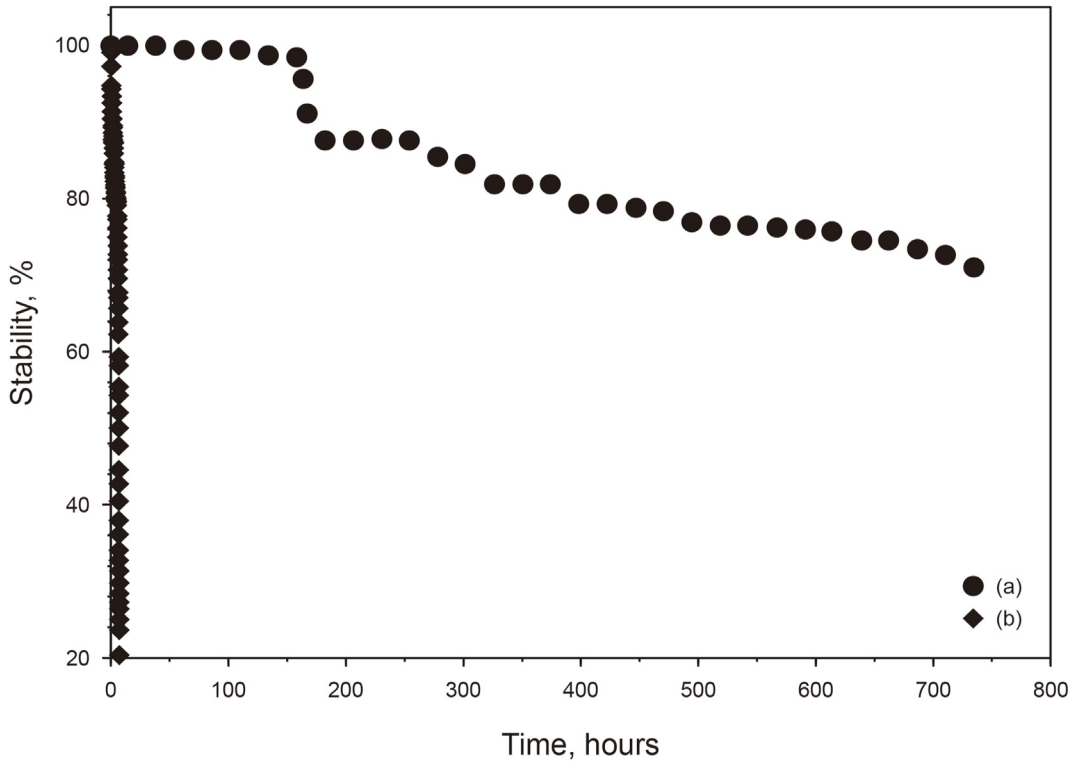

Fig. 15. Stability of foams produced by connate water 1 containing 200 ppm of FSS(β) at (a) reservoir conditions of 150 °C and 2,000 psi, and (b) 70 °C and atmospheric pressure.

supramolecular surfactant is 7.16 dyn/cm and decreases down to 0.302 dyn/cm when FSS(β) is applied.

3.5. Rheological measurements

In Fig. 17, the relation between the viscosity of the connate water 2 at different concentrations of FSS(β) is shown. Despite the supramolecular aggregation the viscosity increase linearly from 0 ppm to 3,000 ppm with a value from 0.7 to 1.32 mPa·s which is an acceptable increment in viscosity to allow the injection of the additivated brine to the well for the mentioned concentrations.

The foam behaves as a pseudoplastic (Fig. 18), *i.e.*, its viscosity μ

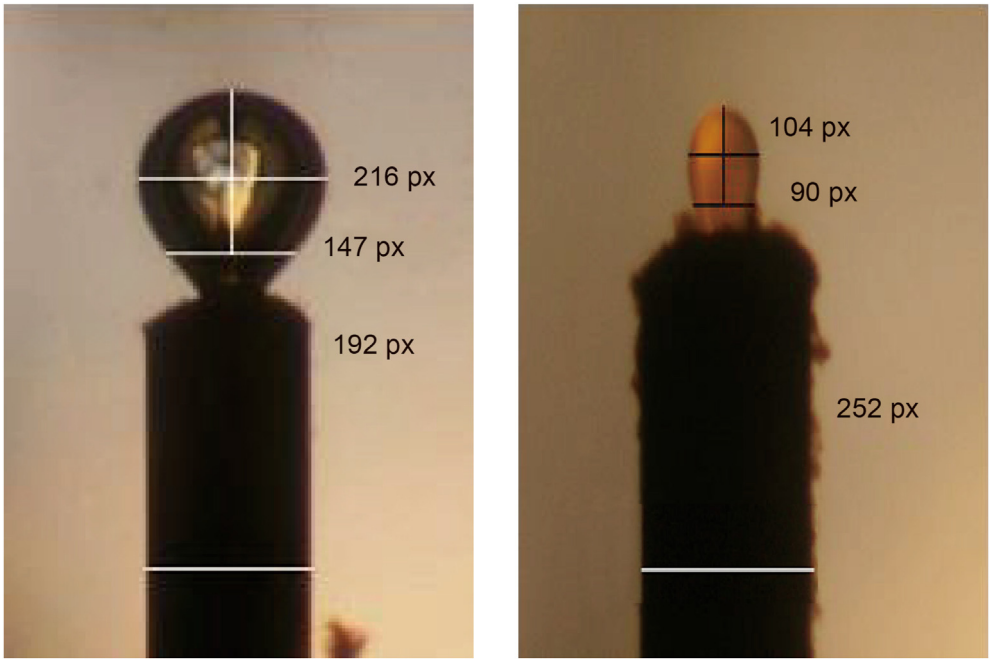

Fig. 16. Experimental results of the relevant dimensions (in pixels) for the interfacial tension measurements at reservoir conditions of 150 °C and 3,500 psi, for (left) the connate water 1/crude oil 1 system, leading to an interfacial tension of 7.16 dyn/cm, and (right) the connate water brine/crude oil 1/600 FSS(β) ppm system, leading to an interfacial tension of 0.302 dyn/cm.

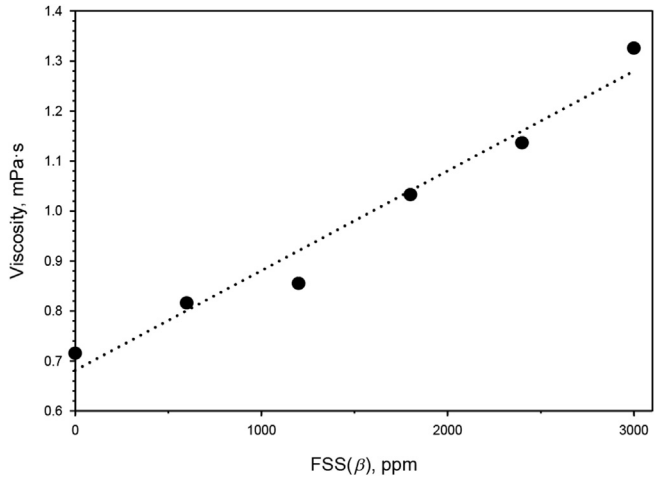

Fig. 17. Viscosity of the connate water 2 containing FSS(β) concentrations among 600 and 3,000 ppm at 70 °C and atmospheric pressure.

decreases with the shear rate γ as

$$\mu = K\gamma^{n-1} \tag{10}$$

where K is the flow consistency index and n is the flow behavior index. The mathematical adjustment of Eq. (10) to the rheological behavior shown in Fig. 20 leads to $K = 428.6$ mPa s and $n = 0.2527$, with a correlation ratio $R^2 = 0.9581$. Pseudoplasticity is the desirable behavior since, at high shear rates, the viscosity is reduced down to one order of magnitude less than at the low shear rate viscosity; then, it is possible to inject the foam at high shear rates to reach the fractured regions, and when the foam velocity decreases at the finish of the injection, the viscosity increases. For example, around 12 s^{-1} (which is a typical velocity in the formation), the foam viscosity is around 64 mPa s (Fig. 20), that is, 300 times higher than the brine viscosity at reservoir conditions, or 2,700 higher than the nitrogen viscosity; so, the FSS(β)-containing connate water 2 would be the phase with the least mobility in the permeable media.

3.6. Core flood experiments

The differential pressure increases linearly as a function of the injection flow rate of nitrogen along with the connate water 2 either at irreducible saturation or containing 600 ppm of FSS(β) (Fig. 19); this fact indicates that at the experimental conditions, the flow behavior through porous medium lies in the Darcy regime.

The increment in the pressure drop when nitrogen is injected along with saturated irreducible connate water 2 demonstrates a higher resistance to the fluid flow, but the core is occluded by the foam formed by the FSS(β)-containing connate water 2/nitrogen mix, as the differential pressure produced by the injection of latter confirms since is greater than 10 times the one produced by the injection of the nitrogen/connate-water mix without foaming.

To determine the resistance factor the drop pressure against flow rate was evaluated for the core without surfactant and with a surfactant, for every flow rate the drop pressure was monitored until it remains constant, usually after 1 or 1.5 pore volumes of the injected nitrogen, and the same procedure was performed for the case of the core with oil. In Fig. 20, the comparison of the foam resistance factor without the presence of oil and with oil is presented, it is observed that the resistance factor decreases in the presence of oil, likewise, the resistance factor also decreases as the nitrogen injection flow rate increases, *i.e.*, as the shear rate increases inside the core.

At a high injection flow rate, the low foam resistance enables adequate injectivity, either in the presence or absence of oil. On the

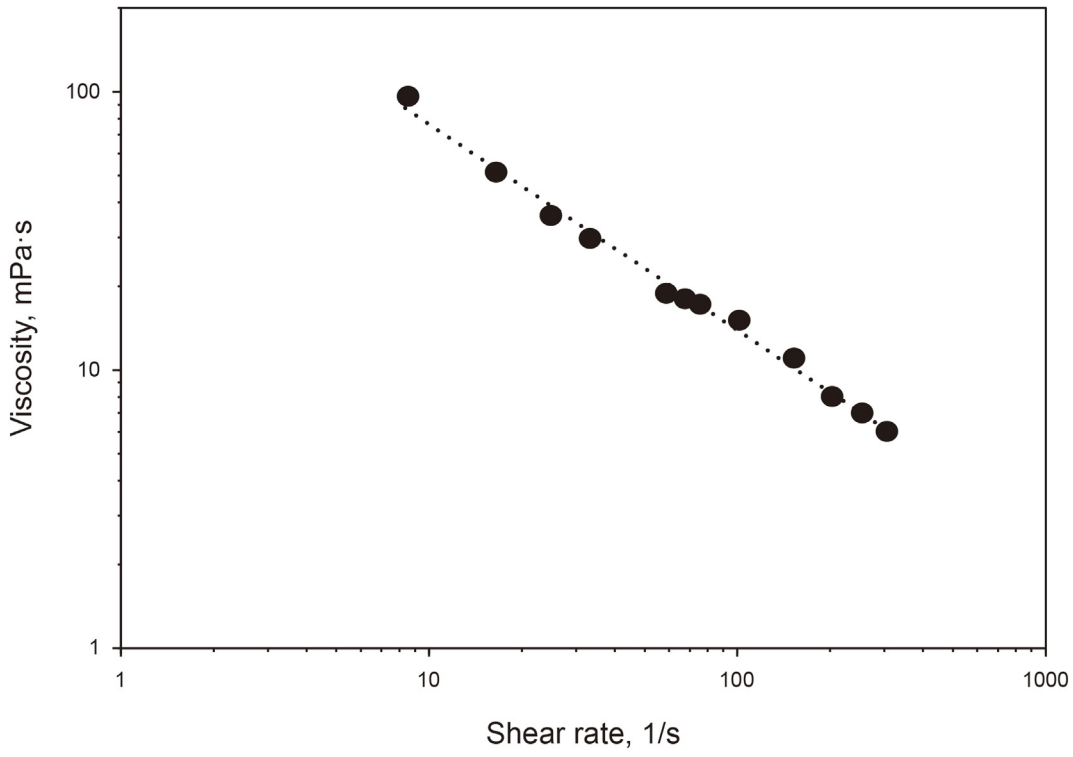

Fig. 18. Viscosity of the foam formed with 600 ppm of FSS(β) in connate water 2, 80% of foam quality, under 3,500 psi and at 150 °C.

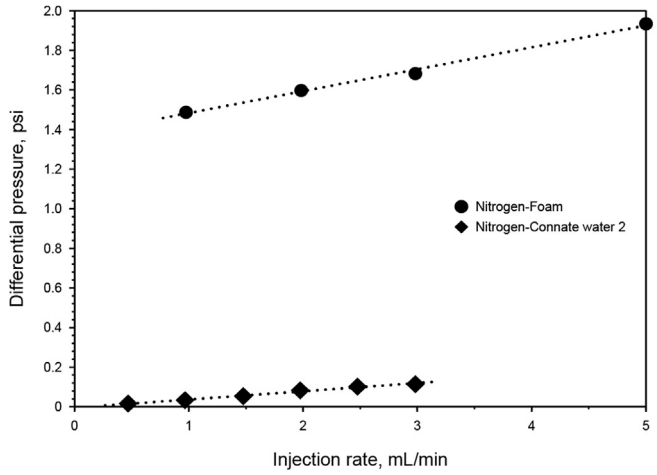

Fig. 19. Comparison of the differential pressure at several injection rates of nitrogen along with the connate water 2 at irreducible saturation in the porous medium (blue circles), and with the connate water 2 containing 600 ppm of FSS(β) (green circles).

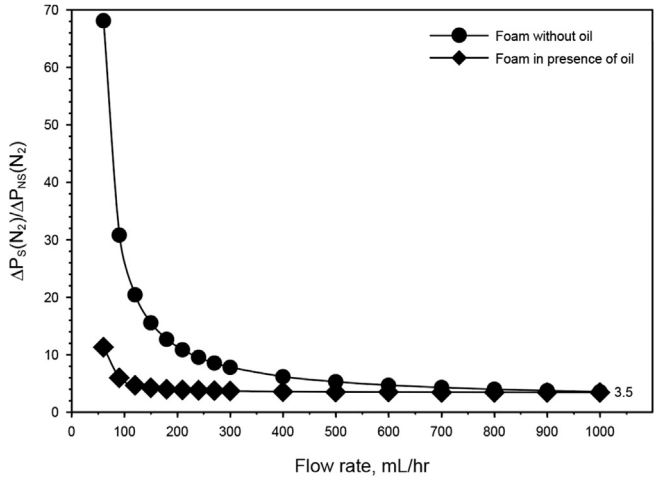

Fig. 20. Gas block factor for the foam generated under 3,500 psi at 150 °C with the connate water 2 containing 600 ppm of FSS(β), as a function of the injected nitrogen flow rate. Green circles: foam in the presence of oil; blue circles: foam without oil. The subscripts S and NS refer to the use of surfactant and non-surfactant presence.

other hand, at a low injection flow rate, the viscosity of the foam increases, therefore its resistance increases, and consequently the injectivity decreases. Once the foam is confined in-situ, it blocks the gas flow within the formation, mainly at the high permeability zones where it is specifically placed, thus enabling more influx from low permeability zones where the oil is located. At a high injection flow rate, the foam resistance factors for oil-saturated and oil-unsaturated cores are equal. This indicates that the fluid velocity is the main parameter influencing the resistance factor at large shear rates. In contrast, at lower velocities, the foam resistance factor is less for the case with oil than without oil, which suggests that oil will be able to pass through the foam-containing regions due to a foam destruction mechanism when foam contacts oil, while the oil-free regions remain blocked.

The above methodology can be used to design huff and puff field applications, where the behavior of the foam is measured during both its early injection and the later production phase once the well is open. For this purpose, it is important to identify the desirable chemical characteristics of the supramolecular surfactant to achieve the best performance under the reservoir conditions of pressure, temperature, salinity, and hardness, as well as to drive the non-Newtonian rheology that provides adequate injectivity properties, on the one hand, of low viscosity at large shear rates, as during foam injection, and on the other, of high viscosity at low velocities, as usually encountered deep into the reservoir, where the supramolecular surfactant serves as a gas barrier in high permeability zones.

4. Conclusions

It is presented a study on the foaming behavior and application of a new hydroxisultaine-based supramolecular surfactant, which is capable of withstanding high salinity, pressure, and temperature conditions, overcoming the performance of commercial foaming agents and betaine-based foaming agents commonly already applied in the field of gas control.

The quantum theoretical modeling drove the design of the functionality of the foaming supramolecular surfactants to activate the preliminary formation of supramolecular monomers. Inside an aqueous environment, those supramolecular monomers containing hydroxysultaine-based surfactants are less stable than those containing betaine-based ones due to the major polarity, but this polarity allows to take advantage of the divalent cations to form premicelles with stronger cohesion, which grow up to form oligomers leading to more stable foams that tolerate the high pressure, high temperature, and exceptionally high hardness and high salinity of the reservoir.

The experimental results indicate that the rheological behavior of the foam is responsible for the ability to be injected into the reservoir at high shear rates and the capability to block the gas, once the foam is placed in the formation fractures where the shear rate decreases.

Additionally, it is important to note that due to the supramolecular assembly, the hydroxysultaine-based surfactants can be manipulated to achieve the best cost-benefit ratio in their production. It is particularly worthy to mention the low negative impact of these surfactants on the environment, which is a requirement for these types of products nowadays. Finally, it is also important to remark that the FSS was successfully tested in a technological field test and approved by a Mexican oil operator.

Acknowledgments

The authors want to acknowledge the supports granted by Instituto Mexicano del Petróleo (IMP) through the Project Y.00123 “Procesos de RM en yacimientos carbonatados fracturados de alta salinidad y temperatura con base en el diseño, desarrollo y escalamiento de productos químicos ad hoc”, which was financially supported by the SENER-CONACYT/Hidrocarburos fund through the Project 146735, D.61029 “Diseño y síntesis de nuevos prototipos de productos químicos multifuncionales con propiedades dispersantes de asfaltenos modificadoras de la mojabilidad y desemulsificantes”, and H.61057 “Bombeo neumático asistido por agentes espumantes multifuncionales de tecnología IMP”. Likewise, R. C. C., E. S. C. and R. C. D. also wish to thank the Dirección de Cátedras CONACyT for his appointment.

References

Accelrys Software Version 7.0, Inc, 2012. http://www.accelrys.com/. (Accessed 6 April 2022).

AlYousef, Z., Ayirala, S., Gizzatov, A., et al., 2020. Evaluating foam stability using tailored water chemistry for gas mobility control applications. J. Pet. Sci. Eng. 195, 1–7. https://doi.org/10.1016/j.petrol.2020.107532.

Amro, M., Finck, M., Jaeger, P., 2015. Foams at Elevated Pressure in EOR. OnePetro, https://doi.org/SPE-172712-MS.

Bergner, A., Dolg, M., Küchle, W., et al., 1993. Ab initio energy-adjusted pseudopotentials for elements of groups 13–17. Mol. Phys. 80, 1431–1441. https://doi.org/10.1080/00268979300103121.

Bouquet, S., Douarche, F., Roggero, F., et al., 2020. Foam processes in naturally fractured carbonate oil-wet reservoirs: technical and economic analysis and optimization. J. Pet. Sci. Eng. 190, 0920–4105. https://doi.org/10.1016/j.petrol.2020.107111.

Bratton, T., Viet Canh, D., Van Que, N., et al., 2006. Schlumberger: La naturaleza de los yacimientos naturalmente fracturados (in Spanish). http://www-wsm.physik. https://www.slb.com/-/media/files/oilfield-review/naturally-fract-reservoirs-2-spanish. (Accessed 6 April 2022).

Chen, P., Mohanty, K.K., 2014. Wettability alteration in high temperature carbonate reservoirs. OnePetro 169125-MS, 12–16. https://doi.org/10.2118/169125-MS.

Chevallier, E., Bouquet, S., Gland, N., et al., 2019. Advanced EOR Foam in Naturally Fractured Carbonates Reservoirs: Optimal Balance between Foam and Interfacial Tension Properties. https://doi.org/10.2118/194992-MS. OnePetro.

Cisneros-Dévora, R., Hernández-Altamirano, R., Martínez-Magadán, J.M., et al., 2020. Development through computational design of a new terpolymer with anti-scale properties applied to the oil production assurance process. Fuel 282, 1–8. https://doi.org/10.1016/j.fuel.2020.118832.

Côté, A.P., Shimizu, G.K.H., 2001. The first example of a functional pillared metal sulfonate network. Chem. Commun. (J. Chem. Soc. Sect. D) 3, 251–252. https://doi.org/10.1039/B005923O.

Danzik, M., 1993. Viscosity Control Additives for Foaming Mixtures. US5273682A. https://patents.google.com/patent/US5273682. (Accessed 6 April 2022).

Dolg, M., Wedig, U., Stoll, H., et al., 1987. Energy-adjusted ab initio pseudopotentials for the first row transition elements. J. Chem. Phys. 86, 866–870. https://doi.org/10.1063/1.452288.

Donon, J., Habka, S., Very, T., el al, 2021. Ion pair supramolecular structure identified by ATR-FTIR spectroscopy and simulations in explicit solvent. ChemPhysChem. 22, 2442–2455. https://doi.org/10.1002/cphc.202100565.

Elhassan, M., Keshtta, O.M., Berrim, A., et al., 2019. Design of foam gas shut-off pilot for a giant high-temperature, high-salinity carbonate reservoir. OnePetro 197322-MS, 11–14. https://doi.org/10.2118/197322-MS.

Firoze Akhtar, T., Ahmed, R., Elgaddafi, R., et al., 2018. Rheological behavior of aqueous foams at high pressure. J. Pet. Sci. Eng. 162, 214–224. https://doi.org/10.1016/j.petrol.2017.12.050.

Flores, J.G., De Antunano, Y., Diaz, A., et al., 2011. Stimulation solutions for the high-pressure, high-temperature naturally fractured carbonate reservoirs in Mexico. OnePetro 144183-MS, 7–10. https://doi.org/10.2118/144183-MS.

Flores-Mondragón, J.S., Bernal Huicochea, C.A., Zamudio Rivera, L.S., et al., 2015. Test and first results of an EOR wettability alteration foam injection test in a naturally fractured reservoir. ASME V010T11A027, 1–5. https://doi.org/10.1115/OMAE2015-41446.

Gagné, O.C., Hawthorne, F.C., 2016. Bond-length distributions for ions bonded to oxygen: alkali and alkaline-earth metals. Acta Crystallogr. B B72, 602–625. https://doi.org/10.1107/S2052520616008507.

Grant, D.M., Harris, R.K., 2002. Advances in NMR. Encyclopedia of Nuclear Magnetic Resonance, 9. John Wiley & Sons. Ltd., Chichester.

Han, M., AlSofi, A., Fuseni, A., et al., 2013. Development of chemical EOR formulations for a high temperature and high salinity carbonate reservoir. Soc Pet Eng 17084-MS, 26–28. https://doi.org/10.2523/IPTC-17084-MS.

Hernandez Altamirano, R., Zamudio Rivera, L., Mena-Cervantes, V., et al., 2016. Foaming Composition with Wettability Modifying and Corrosion Inhibitory Properties for High Temperature and Ultra-high salinity.US9469804B2. https://patents.google.com/patent/US9469804. (Accessed 6 April 2022).

Hernández Altamirano, R., Zamudio Rivera, L.S., Mena Cervantes, V.Y., et al., 2020. Multifunctional Foaming Composition with Wettability Modifying, Corrosion Inhibitory and Mineral Scale Inhibitory/dispersants Properties for High Temperature and Ultra High Salinity. US10597578B2. https://patents.google.com/patent/US10597578. (Accessed 6 April 2022).

Kargarpour, M.A., 2020. Carbonate reservoir characterization: an integrated approach. J. Pet Explor. 10, 2655–2667. https://doi.org/10.1007/s13202-020-00946-w.

Katz, A.K., Glusker, J.P., Beebe, S.A., et al., 1996. Calcium ion coordination: a comparison with that of beryllium, magnesium, and zinc. J. Am. Chem. Soc. 118, 5752–5763. https://pubs.acs.org/doi/abs/10.1021/ja953943i.

Klamt, A., Schüürmann, G., 1993. COSMO: a new approach to dielectric screening in solvents with explicit expressions for the screening energy and its gradient. J. Chem. Soc. 5, 799–805. https://doi.org/10.1039/P29930000799.

Le, L.Q., Ramanathan, R., Nasr-El-Din, H.A., 2019. Evaluation of an ethoxylated amine surfactant for CO_2-foam stability at high salinity conditions. OnePetro 197515-MS, 11–14. https://doi.org/10.2118/197515-MS.

LENNTECH, 2022. Periodic Table. https://www.lenntech.com/periodic/periodic-chart.htm. (Accessed 6 April 2022).

Li, T., Fang, J., Jiao, B., et al., 2018. Study on a novel gelled foam for conformance control in high temperature and high salinity reservoirs. MDPI 11(6), 1364–1370. https://doi.org/10.3390/en11061364.

Liu, R., Yu, T., Shi, Z., et al., 2016. The preparation of metal-organic frameworks and their biomedical application. Int. J. Nanomed. 11, 1187–1200. https://doi.org/10.2147/IJN.S100877.

Lu, J., Goudarzi, A., Chen, P., et al., 2014. Enhanced oil recovery from high-temperature, high-salinity naturally fractured carbonate reservoirs by surfactant flood. J. Pet. Sci. Eng. 124, 122–131. https://doi.org/10.1016/j.petrol.2014.10.016.

Mohamed, A.I.A., Sultan, A.S., Hussein, I.A., et al., 2017. Influence of surfactant structure on the stability of water-in-oil emulsions under high-temperature high-salinity conditions. J. Chem. 2017, 1–12. https://doi.org/10.1155/2017/5471376.

Onoda, A., Yamada, Y., Doi, M., et al., 2001. Dinuclear calcium complex with weakly NH···O hydrogen-bonded sulfonate ligands. Inorg. Chem. 40(3), 516–521. https://pubs.acs.org/doi/abs/10.1021/ic0003067.

Ortmann, F., Bechstedt, F., Schmidt, W.G., 2006. Semiempirical van der Waals correction to the density functional description of solids and molecular structures. Phys. Rev. B 73, 205101–205109. https://doi.org/10.1103/PhysRevB.73.205101.

Parra, J.E., Rosales Arias, F., Soto-Castruita, E., et al., 2020a. Multifunctional Foaming Agents for Production Enhancement in Oil Wells: Field Test Results. https://doi.org/10.2118/201648-MS. OnePetro.

Parra, J.E., Soto-Castruita, E., Cerón-Camacho, R., et al., 2020b. Design and Evaluation of Multifunctional Foaming Agents for Production Enhancement in Oil Wells. https://doi.org/10.2118/201603-MS. OnePetro.

Pérez-Alvarez, M., Oviedo-Roa, R., Soto-Castruita, E., et al., 2018. Growth inhibition in calcium sulfate crystal using a copolymer in oil fields: theoretical study and experimental evaluations. Iran. Polym. J. (Engl. Ed.) 27, 927–937. https://doi.org/10.1007/s13726-018-0663-0.

Pons-Jiménez, M., Hernández-Altamirano, R., Cisneros-Dévora, R., et al., 2015. Theoretical and experimental insights into the control of calcium sulfate scales by using random copolymers based on itaconic acid. Fuel. 149, 66–77. https://doi.org/10.1016/j.fuel.2014.09.064.

Rasheed, K., Cravey, R., Berger, P.D., et al., 1991. Alkoxylated Alkyl Substituted Phenol Sulfonates Compounds and Compositions, the Preparation Thereof and Their Use in Various Applications. US5049311A. https://patents.google.com/patent/US5049311. (Accessed 6 April 2022).

Sandrea, R., 2019. Understanding the Challenges to Mexico's Oil & Gas Future. https://eprinc.org/wp-content/uploads/2019/07/Sandrea-Mexico-Paper-July-2019-FINAL-1.pdf. (Accessed 6 April 2022).

Schalley, C., 2007. Analytical Methods in Supramolecular Chemistry. Wiley-VCH Verlag GmbH & Co. KGaA. https://doi.org/10.1002/9783527610273.

Skauge, A., Aarra, M.G., Ormehaug, P., et al., 2019. Preparations for foam gas shut off in carbonate reservoirs. OnePetro 197640-MS, 11–14. https://doi.org/10.2118/197640-MS.

Vosko, S.H., Wilk, L., Nusair, M., 1980. Accurate spin-dependent electron liquid correlation energies for local spin density calculations: a critical analysis. Can. J. Phys. 58, 1–7. https://doi.org/10.1139/p80-159.

Wang, D., Sun, J., 2019. Oil recovery for fractured-vuggy carbonate reservoirs by cyclic water huff and puff: performance analysis and prediction. Nature. 9, 15231–15238. https://doi.org/10.1038/s41598-019-51807-4.

Wang, Y., Zhang, Y., Liu, Y., et al., 2017. The stability study of CO_2 foams at high pressure and high temperature. J. Pet. Sci. Eng. 154, 234–243. https://doi.org/10.1016/j.petrol.2017.04.029.

Wu, X., Yang, Z., Xu, H., et al., 2016. Success and lessons learned from polymer-flooding a ultra high temperature and ultra high salinity oil reservoir - a case study from West China. OnePetro 179594-MS, 11–13. https://doi.org/10.2118/179594-MS.

Xu, Z.X., Li, S.Y., Li, B.F., et al., 2020. A review of development methods and EOR technologies for carbonate reservoirs. Petrol. Sci. 17, 990–1013. https://doi.org/10.1007/s12182-020-00467-5.

Zamudio Rivera, L.S., López Ramírez, S., Durán, V.C.D.L.Á., et al., 2014. Foaming Composition for High Temperature and Salinity. US8722588B2. https://patents.google.com/patent/US8722588. (Accessed 6 April 2022).

Zhang, X., Wang, C., 2011. Supramolecular amphiphiles. Chem. Soc. Rev. 40, 94–101. https://doi.org/10.1039/B919678C.

Zhang, H., Miller, C.A., Garrett, P.R., et al., 2003. Mechanism for defoaming by oils and calcium soap in aqueous systems. J. Colloid Interface Sci. 263, 633–644. https://doi.org/10.1016/S0021-9797(03)00367-9.